electronics

Article

Voltage and Current Sensor Fault Diagnosis Method for Traction Rectifier in High-Speed Trains

Yunjun Yu [1,2], Yunquan Song [1], Hongwei Tao [1,*] and Jiawen Hu [1]

[1] School of Information Engineering, Nanchang University, Nanchang 330031, China
[2] Institute of Industrial Artificial Intelligence, Nanchang University, Nanchang 330031, China
* Correspondence: hongweitao@ncu.edu.cn

Abstract: The traction rectifier plays a key role in high-speed trains. Unexpected failure often occurs in the sensors of the rectifier, which may affect the control performance of the electric traction rectifier and even cause serious deterioration to high-speed trains. A sensor fault diagnosis method is presented in this paper, considering three kinds of common fault types. It can not only locate the sensor fault, but also identify fault types. Based on the influences of the sensor faults, the fault diagnosis thresholds can be calculated quantitatively. No additional hardware is required. First, the model of the rectifier is established, and the estimator is built. The current residuals with different faults can be obtained. Next, residuals are analyzed and features are acquired. Then, diagnosis functions are constructed, which are used for fault location and fault type identification. Finally, the feasibility and effectiveness of the method have been confirmed by the experimental results.

Keywords: fault diagnosis; traction rectifier; current sensor fault; voltage sensor fault

check for updates

Citation: Yu, Y.; Song, Y.; Tao, H.; Hu, J. Voltage and Current Sensor Fault Diagnosis Method for Traction Rectifier in High-Speed Trains. *Electronics* **2024**, *13*, 197. https://doi.org/10.3390/electronics13010197

Academic Editor: Ahmed Abu-Siada

Received: 25 November 2023
Revised: 23 December 2023
Accepted: 28 December 2023
Published: 2 January 2024

Copyright: © 2024 by the authors. Licensee MDPI, Basel, Switzerland. This article is an open access article distributed under the terms and conditions of the Creative Commons Attribution (CC BY) license (https://creativecommons.org/licenses/by/4.0/).

1. Introduction

With the recent rapid development of high-speed trains, their reliability has received increasing attention [1–3]. A typical AC/DC/AC traction converter used in high-speed trains is shown in Figure 1; it consists of a grid-side two-level rectifier and a motor-side three-phase inverter [4]. It also contains a control unit and circuit. In such a traction converter, every part plays a key role, and the motor-side inverter is in charge of the control induction machines. The whole traction system relies on the reliability of the rectifier [5,6]. Because of the destructiveness and high rate of rectifier failure, it has been paid much attention recently. Nevertheless, most of the research published in the past few years has been about transistor faults [7]. The accuracy of the feedback signals collected and provided by sensors deeply influences the control unit of the system [8]. Due to the complex operating conditions, such as humidity, temperature, and static electrical corrosion, unexpected failures may occur in sensors [9], which may lead to signals' deviation provided by sensors and even the catastrophic subsequent failure of high-speed trains [10,11]. Therefore, methods that are capable of detecting and diagnosing different sensor faults have application value and are of great significance for rectifiers.

Sensor fault diagnosis methods can be classified into three types—signal-based [12,13], data-driven [14–16], and model-based methods [17–19]. In signal-based methods, signal characteristics are usually extracted as evidence of fault diagnosis. They can be applied to systems that are difficult to model mathematically. In [20], a method was proposed for the current sensor fault; this signal-based method can detect and tolerate the faults. The integrated frame based on the premise of the analysis of fault modes was built for current sensors. The fault can be located according to the sum value of three currents. Although it has been demonstrated that this method can detect and tolerate three kinds of faults, it could not identify which kind of fault occurs. In addition, there are two stator current sensors in most real systems due to cost saving. By comparing the measured value

with the delayed rotor speed signals, the position sensor fault can be located in [21]. Then, alternative position estimators are built for the tolerant control approach. On the one hand, signal-based methods do not need a mathematical model, since the features of the signals can be extracted and used for fault diagnosis directly. On the other hand, signal-based methods often need large actual calculation and deduction, and extra sampling circuits are often required. Data analytics techniques have been widely applied in many fields in recent years. The data-driven methods can ignore the traction system model. Thus, they can be used in those systems that have complicated topology. A historical database is usually set up, which saves a great amount of data of the system in healthy and faulty states. The hidden information can be acquired by learning historical data by means of statistical analysis, artificial intelligence, etc. In [14], a data-driven approach successfully diagnosed the sensor faults for the traction system. The extreme learning machine in this paper has been trained on data set learning, and the ensemble extreme learning machine classifier built in the paper can effectively decrease the error. Usually, data-driven methods have better robustness to the system than other methods in environments with high noise. Nevertheless, a great deal of data are required. These methods are not easy to apply to real-time diagnosis, for they usually spend a longer time in fault diagnosis. Thus, for now, data-driven methods are not suitable for fast traction system sensor fault real-time diagnosis.

In model-based methods, models of practical systems need to be built; the fault is diagnosed according to the difference of signals in the system and the model. Most studies focus on the sensors in the motor side of the traction system, such as the speed and current sensors. Ref. [22] proposes a joint fault diagnosis method for speed and broken rotor bar sensors based on unknown input observers. The sliding mode observer and interval observer are constructed for the subsystems decoupled from the traction system. Diagnosis methods for voltage and current sensors are essential. The widely used methods are based on an adaptive observer, an extended Kalman filter, a model reference adaptive system observer, etc. In [23], a diagnosis method for voltage sensor and power transistor devices faults is proposed; the residual generation applied to fault diagnosis is acquired by the measured value, subtracting the observed current. The residual is also provided with an adaptive threshold. However, the grid current sensor faults have not been considered. A fault diagnosis and system reconfiguration strategy is presented in [24]. It relies on the sliding mode observer for the traction rectifier. A novel fault-tolerant strategy is proposed. Although the paper validates the effectiveness of the method under three kinds of fault, it could not identify fault types after the fault is detected. Additionally, the conditions of the voltage sensor have not been considered. In [25], a sensor fault detection and isolation approach with control reconfiguration has been proposed. Both DC side voltage and current sensors are included; the Luenberger observer consisted of a voltage sensor fault and the open loop estimator was developed. Although both the current and voltage sensor faults can be diagnosed based on observers and residual generation, four residuals are established. The above two methods cannot recognize the type of sensor fault. The residuals consisting of the line and phase voltage have been applied to current sensor fault diagnosis in [26]. However, in the real traction system, the line and phase voltage sensors are not often used. In [27], in order to decrease the diagnosis time, a method based on the sum deviation of three inductor currents was developed. However, there are two inductor current sensors in most real traction systems in order to save costs. In [28], a sensor fault diagnosis and isolation approach for DC link voltage applied to a three-level rectifier is presented, which combines sliding mode technique. In order to improve the robustness of the method, the nonlinear parametrization adaptive estimation was applied; this method is not suitable for the two-level converter, and the current sensor fault and fault type identification are not taken into consideration. In [29], a real-time fault diagnosis method is presented; this method could diagnose the sensor fault in the rectifier. However, this will increase the cost due to the method needing an additional voltage sensor. Scaling, offset, and drift faults

are common in sensors [30,31]. Fault diagnosis for sensors still needs to be investigated to improve the reliability of trains.

A fault diagnosis method for sensors in traction rectifiers has been put forward. Both catenary current and DC link voltage sensors can be diagnosed. In addition, the proposed method has the ability to identify fault type. The common sensor faults are taken into account. No extra sensor is needed, which can save on costs. The rest of this article is organized as follows. The rectifier model is presented in Section 2. In Section 3, fault types are introduced. In Section 4, the estimator is constructed, the residual is acquired and analyzed, and the detection and diagnosis functions are constructed. The experimental results are shown in Section 5. Section 6 concludes this article.

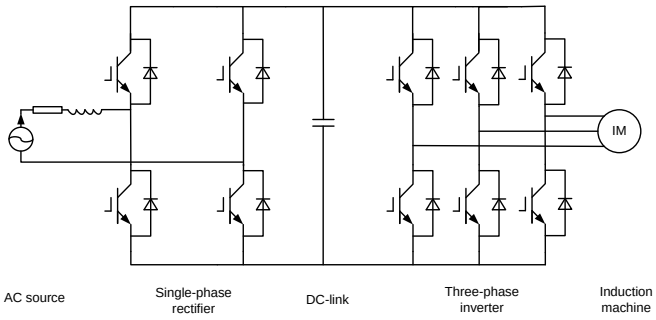

Figure 1. Topology of two-level converter.

2. System Description

The topology of the single-phase rectifier circuit is shown in Figure 2. There are two legs in the rectifier. T_{x1}, T_{x2} stand for insulated gate bipolar transistors (IGBTs) in x-leg, and D_{x1}, D_{x2} stand for freewheeling diodes; x in these described symbols could be a and b. On the grid side, L_n and R_n denote the traction winding leakage inductance and resistance, respectively. u_n represents the grid voltage and i_n is the grid current, which is measured by the current sensor of S_{Cn}. C is the support capacitor and R_1 is the load. u_{dc} is the DC link voltage; it also denotes the voltage of the capacitor and it is measured by the voltage sensor of S_{Vd}.

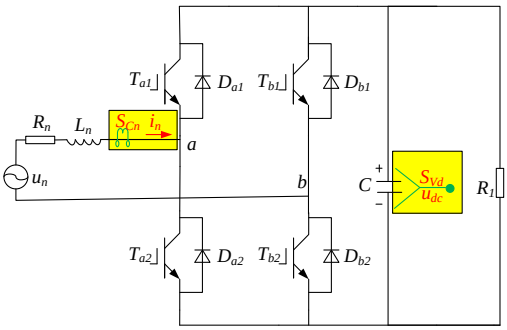

Figure 2. Topology of the single-phase rectifier circuit.

Switching devices in the above traction rectifier can be assumed to work as ideal switches, the deadtime can be ignored, and the switching functions used for describing the switches' states can be expressed.

$$S_x = \begin{cases} 1, & T_{x1} \text{ on or } D_{x1} \text{ on} \\ 0, & T_{x2} \text{ on or } D_{x2} \text{ on} \end{cases}. \tag{1}$$

According to (1), the input voltage of the rectifier can be obtained:

$$u_{ab} = (S_a - S_b)u_{dc}. \tag{2}$$

The state space equation of the two-level traction rectifier can be constructed according to Kirchhoff's voltage law:

$$u_n = L_n \frac{di_n}{dt} + R_n i_n + (S_a - S_b)u_{dc}. \tag{3}$$

3. Fault Analysis

Of all the sensor faults in traction systems, the offset, scaling, and drift faults have high incidence and have been taken into account. When an offset fault occurs, there will be extra value on the actual value. When a scaling fault occurs, there is a scaling gain between the measured value output by the sensors and the actual value. When drift fault occurs, there is a superimposed value that changes with time on the actual value. As described above, these kinds of faults can be defined as follows:

$$V_{meas} = V_{actu} + \delta \tag{4}$$

$$V_{meas} = c_{sca} V_{actu} \tag{5}$$

$$V_{meas} = V_{actu} + c_{dri} \cdot \Delta t, \tag{6}$$

where V_{meas} is the measured value and V_{actu} is the actual value; δ, c_{sca}, and c_{dri} are the offset value, scaling factor, and drift factor, respectively. For voltage sensor faults, because the effect of the scaling fault is the same as that of the offset fault, only the offset fault of the voltage sensor is taken into account in this article. The factor of the scaling fault in S_{Cn} is set to be 1.5, the offset value of the current sensor is 2 A, the factor of the offset fault in S_{Vd} is set to be 20, and the drift factor is 80 in this paper.

4. Fault Detection and Diagnosis

4.1. Residual Generation

The residual constructed in this paper is a suitable candidate for fault diagnosis. According to (3), the two-level rectifier state estimator is given by:

$$u_n = L_n \frac{d\hat{i}_n}{dt} + R_n \hat{i}_n + (S_a - S_b)u_{dc}, \tag{7}$$

where $\hat{i}_n$ is the estimator value of the grid current. Then, combined with the measured value, the system residual is defined as:

$$\tilde{i}_n = i_n - \hat{i}_n. \tag{8}$$

The residual of the current is nearly 0 when the rectifier works in normal conditions. After a fault occurs, it will significantly change.

4.2. Fault Detection

According to the above analysis, $\tilde{i}_n$ changes obviously when a sensor fault occurs. The signal of $\tilde{i}_n$ is sampled, $\tilde{i}_n(k)$ is the value of $\tilde{i}_n$ at the k moment. $F_1(k)$ is given for sensor fault detection:

$$F_1(k) = \begin{cases} 1, & \tilde{i}_n(k) > K_0 \\ -1, & \tilde{i}_n(k) < -K_0 \end{cases}, \tag{9}$$

where K_0 is the threshold of $F_1(k)$.

The average of $|F_1(k)|$ in a period of a system is given as

$$D(k) = \frac{1}{M}[\sum_{j=k-M+1}^{k} |F_1(j)|]. \tag{10}$$

where M is the sampling number in a period. The sensor fault is detected according to the function of $D(k)$.

$$E(k) = \begin{cases} 1, & D > h_0 \\ 0, & D < h_0 \end{cases}, \tag{11}$$

where h_0 is the threshold, $E(k) = 1$ denotes that the sensor fault has been detected. $E(k) = 0$ represents when no faults have occurred in the sensor.

4.3. Fault Diagnosis

It can be seen that i_n is approximately equal to $\hat{i}_n$ when the system works normally. After the occurrence of a scaling fault in S_{Cn}, i_n changes to $c_{sca}i_n$. Then, $\tilde{i}_n$ is expressed as:

$$\tilde{i}_n = (c_{sca} - 1)i_n. \tag{12}$$

Thus, the phases of i_n and $\tilde{i}_n$ are the same or opposite after the occurrence of the scaling fault in S_{Cn}.

When there is an offset fault in S_{Cn}, i_n changes to $i_n + \delta$. Then, $\tilde{i}_n$ can be given as:

$$\tilde{i}_n = \delta. \tag{13}$$

It can be seen that $\tilde{i}_n$ is a constant value after the occurrence of an offset fault in S_{Cn}.

When a drift fault occurs in S_{Cn}, i_n changes to $i_n + c_{dri} \cdot \Delta t$. Then, $\tilde{i}_n$ can be can be expressed as:

$$\tilde{i}_n = c_{dri} \cdot \Delta t. \tag{14}$$

It can be seen that $\tilde{i}_n$ will be the ramp function after the occurrence of a drift fault in S_{Cn}.

In the condition of fault in S_{Vd}, the signal provided by S_{Vd} is influenced, and u_{dc} will change to u'_{dc}. The residual of the system can be rewritten by a differential equation.

$$\dot{\tilde{i}}_n = -\frac{R_n}{L_n}\tilde{i}_n + \frac{S_a - S_b}{L_n}(u'_{dc} - u_{dc}). \tag{15}$$

According to Equations (3) and (15), i_n and $\tilde{i}_n$ can be calculated as:

$$i_n = C_1 e^{-\frac{R_n}{L_n}t} + e^{-\frac{R_n}{L_n}t} \int_0^t \frac{1}{L_n}(u_n - u_{ab}) e^{\frac{R_n}{L_n}t}\, dt. \tag{16}$$

$$\tilde{i}_n = \begin{cases} C_2 e^{-\frac{R_n}{L_n}t} + e^{-\frac{R_n}{L_n}t} \int_0^t \frac{S_a - S_b}{L_n}(u'_{dc} - u_{dc}) e^{\frac{R_n}{L_n}t}\, dt, & t < t_0 \\ C_3 e^{-\frac{R_n}{L_n}t} + e^{-\frac{R_n}{L_n}t} \int_{t_0}^t \frac{S_a - S_b}{L_n}(u'_{dc} - u_{dc}) e^{\frac{R_n}{L_n}t}\, dt, & t > t_0 \end{cases}, \tag{17}$$

where C_1, C_2, and C_3 are the coefficients of the functions and depend on the initial condition. Supposing the rectifier began to work normally from $t = 0$, substituting $\tilde{i}_n = 0$ $(t = 0)$ into (17), and the voltage sensor faults occur at t_0. C_2 can be obtained by solving (17) and $C_2 = 0$. C_3 can be acquired according to the limit of $\tilde{i}_n$, when $t = t_0$, $C_3 = 0$.

$$\tilde{i}_n = e^{-\frac{R_n}{L_n}t} \int_{t_0}^t \frac{S_a - S_b}{L_n}(u'_{dc} - u_{dc}) e^{\frac{R_n}{L_n}t}\, dt (t > t_0). \tag{18}$$

One can see that the integrator of (13) and (15) determine the phases of i_n and $\tilde{i}_n$, respectively, when offset fault occurs, $u'_{dc} = u_{dc} + \delta$, δ is the offset factor.

$$\frac{1}{L_n}u_n - \frac{S_a - S_b}{L_n}u_{dc} = \frac{1}{L_n}(u_n - u_{ab}) \tag{19}$$

$$\frac{S_a - S_b}{L_n}(u'_{dc} - u_{dc}) = \frac{\delta}{L_n u_{dc}}u_{ab}. \tag{20}$$

In order to analyze the phase difference clearly, i_n is expressed as $i_n = \sqrt{2}I_n \cos(\omega t + \psi_i)$. I_n, ω, and ψ_i are the effective value, the grid voltage angular frequency in the rectifier, and the initial phase, respectively. Then, $u_n - u_{ab}$ and u_{ab} are vectorized and given as:

$$\dot{U}_n - \dot{U}_{ab} = A_1 \angle(\psi_i + \arctan\frac{\omega L_n}{R_n}) \tag{21}$$

$$\dot{U}_{ab} = A_2 \angle(\psi_i - \arctan\frac{\omega I_n L_n}{U_n - I_n R_n}), \tag{22}$$

where $A_1 = (R_n I_n)^2 + (\omega I_n L_n)^2$ $A_2 = (U_n - R_n I_n)^2 + (\omega I_n L_n)^2$. The phase difference can be calculated as:

$$\angle\phi_i = \arctan\frac{\omega L_n}{R_n} + \arctan\frac{\omega I_n L_n}{U_n - I_n R_n}, \tag{23}$$

where $\angle\phi_i$ is the phase difference and can be calculated as 83.17° when substituting system parameters into (23). Thus, it can be seen that there is a phase difference between i_n and $\tilde{i}_n$ when scaling or offset fault occurs in S_{Vd} of the traction rectifier.

When the drift fault occurs in S_{Vd}, $u'_{dc} = u_{dc} + c_{dri}\Delta t$, where c_{dri} is the drift factor.

$$\tilde{i}_n = e^{-\frac{R_n}{L_n}t}\int_{t_0}^{t}\frac{c_{dri}}{L_n u_{dc}}u_{ab}(t - t_0)e^{\frac{R_n}{L_n}t}\,dt(t > t_0). \tag{24}$$

Similarly, It can be deduced that there is a phase difference between i_n and $\tilde{i}_n$ when a drift fault occurs in S_{Vd}. Additionally, the amplitude of $\tilde{i}_n$ increases with time after the fault occurs.

In order to diagnose the fault, the signal of i_n is sampled. $i_n(k)$ in this paper represents the k instant value of i_n. The function of $F_2(k)$ is defined as follows for sensor fault diagnosis:

$$F_2(k) = \begin{cases} 1, & i_n(k) > K_1 \\ -1, & i_n(k) < -K_1 \end{cases}, \tag{25}$$

where K_1 is the threshold. $P_1(k)$ is given as:

$$P_1(k) = \frac{1}{M}[|\sum_{j=k-M+1}^{k}F_1(j)F_2(j)| - |\sum_{j=k-M+1}^{k}F_1(j)|]. \tag{26}$$

According to the value of P_1, the fault can be located. The relationship between P_1 and the fault location is shown as follows:

$$\begin{cases} h_2 < P_1 < h_1, & \text{Fault in } S_{Vd} \\ \text{other}, & \text{Fault in } S_{Cn} \end{cases}, \tag{27}$$

where h_1 and h_2 are the thresholds. For the proposed identification of fault type, the average of $\tilde{i}_n$ in half of the period of the system is given as:

$$Q(k) = \frac{1}{M_1}[\sum_{j=k-M_1+1}^{k}|\tilde{i}_n(j)|], \tag{28}$$

where $M_1 = \frac{M}{2}$. The differential of $Q(k)$ is described and discretized as follows:

$$P_2(k) = \frac{Q(k) - Q(k-1)}{t_s}, \tag{29}$$

where t_s is the fundamental sample time of the platform.

After the fault is detected, the signal of $Q(k)$ in the first half of the period is not taken into consideration. In the second half of the period, faults could be diagnosed. The diagnosis rules of the proposed diagnosis method have been explained in detail in Table 1, where h_3 is the threshold for fault-type identification.

Table 1. Fault diagnosis rules.

Fault Diagnosis Rules	Fault Location	Fault Type
$P_1 > h_1$	S_{Cn}	Scaling fault
$P_1 < h_2$; $P_2 < h_3$	S_{Cn}	Offset fault
$P_1 < h_2$; $P_2 > h_3$	S_{Cn}	Drift fault
$h_2 < P_1 < h_1$; $P_2 < h_3$	S_{Vd}	Offset fault
$h_2 < P_1 < h_1$; $P_2 > h_3$	S_{Vd}	Drift fault

4.4. Thresholds Selection

Appropriate thresholds are important for the accuracy and feasibility of the proposed method. For K_0, after the occurrence of an offset fault in S_{Vd}, the amplitude of $\tilde{i}_n$ can be deduced. u_{ab} can be assumed as $A_1 \sin(\omega t + \psi)$ where A_1 and ψ are the amplitude and phase of u_{ab}, respectively. $\tilde{i}_n$ can be rewritten as:

$$\tilde{i}_n = e^{\frac{R_n}{L_n}(t_0 - t)} A \sin(\omega t_0 + \psi - \theta) - A \sin(\omega t + \psi - \theta), \tag{30}$$

where $A = \frac{A_1 \delta \sqrt{R_n^2 + L_n^2 \omega^2}}{u_{dc}(R_n^2 + \omega^2 L_n^2)}$, $\theta = \arctan \frac{\omega L_n}{R_n}$, t_0 is the instant of the fault occurring. It can be seen that there is a deviation in $\tilde{i}_n$, which decreases with time after the offset fault occurs. Meanwhile, the parameter of the electrical components can be acquired. Therefore, the scope of $\tilde{i}_n$ can be deduced, $|\tilde{i_n}| < e^{\frac{R_n}{L_n}(t_0 - t)} A + A$, where A can be calculated as 11.8 when substituting system parameters into (30).

Similarly, amplitudes of $\tilde{i}_n$ can be deduced when other kinds of faults occur in S_{Cn} and S_{Vd}. After the residuals are calculated, the value of K_0 should be smaller than these amplitudes simultaneously. Additionally, K_0 should not be too small and should keep an appropriate margin for the proposed method of reducing the impact of the noise in the system. Similarly, other thresholds can be set in the same way.

5. Experimental Results

A small-scale prototype of the single-phase rectifier is built in a laboratory, which is used to investigate the effectiveness of the sensor fault diagnosis method. Figure 3 shows the prototype platform; it basically comprises the control board, the main circuit, the signal processors, and the driver circuit. The system control is implemented using DSP(TMS320F28335). The load is a 3-phase inverter and an induction machine. The grid current and the DC link voltage are measured by sensors in the platform. The electrical parameters are given in Table 2. The experimental results are displayed afterwards.

Table 2. Parameters of system.

Parameters	Symbol	Value
RMS grid-side voltage	u_n	220 V
Grid inductor	L_n	5 mH
Grid resister	R_n	0.2 Ω
DC-link capacitor	C	2.2 mF
DC-link voltage	u_{dc}	340 V

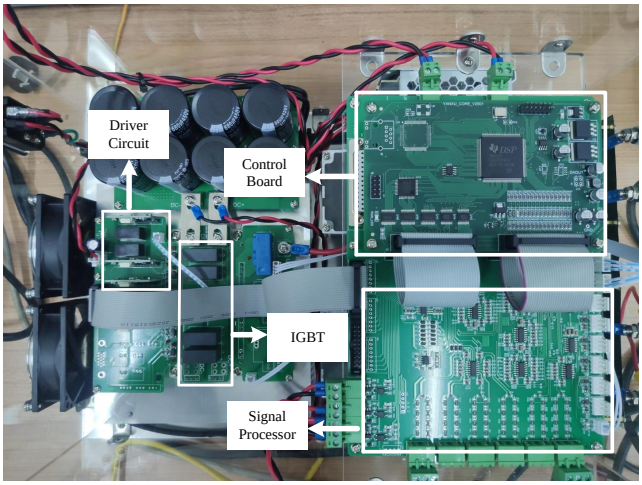

Figure 3. Experimental platform of the test circuit.

When the traction rectifier works in normal conditions, the output of the DC side is 340 V. The amplitude of the grid current is 6A. Due to the residual of $i_n = 0$, the detection function is 0, and the diagnosis functions are 0, too.

In the case when S_{Cn} is in an offset fault, the diagnosis results are shown in Figure 4. It can be seen that, at the instant of t_1 when the system is working normally, the fault occurs. Then, the waveform of u_{dc} decreases from 340 V and its fluctuation becomes larger. i_n almost does not change, which keeps the sine wave with an amplitude of 6 A. Before the fault occurs, $\tilde{i}_n = 0$. $\tilde{i}_n$ increases from 0 to 2 A instantly when the fault occurs. The detection function of D changes from 0 to 1 in a short time. It should be noted that the fault is detected when D surpasses h_0 at t_2. In the second half of the period of the system after the fault is detected, both P_1 and P_2 decrease; P_1 decreases from 0 to -1 and P_2 decreases from 190 to 0. At the time when P_1 is less than h_2 and P_2 is less than h_3 simultaneously, the fault can be diagnosed at t_3.

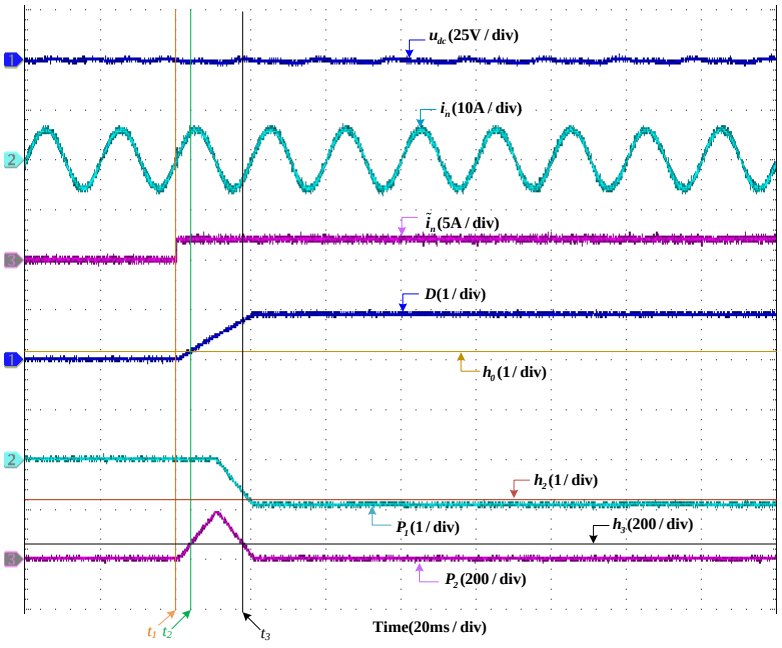

Figure 4. Fault diagnosis results of offset fault occurring in S_{Cn}.

The diagnosis results of S_{Cn} in a drift fault are shown in Figure 5. As is depicted in the picture, the fault occurs at t_1 when the system is working normally. Then, the waveform fluctuation of u_{dc} changes obviously and fluctuates around 340 V. i_n does not change, which keeps the sine wave with an amplitude of 6 A. Before the fault occurs, $\tilde{i}_n = 0$. $\tilde{i}_n$ increases with nearly constant velocity. The detection function of D changes from 0 to 1 in a short time. It should be noted that the fault is detected when D surpasses h_0 at t_2. In the second half of the period, P_2 increases and surpasses h_3. It eventually reaches 90. P_1 decreases from 0 and through the threshold of h_2. It eventually reaches -0.95. According to the diagnosis rules, after a period when a fault has been detected, it can be diagnosed at t_3.

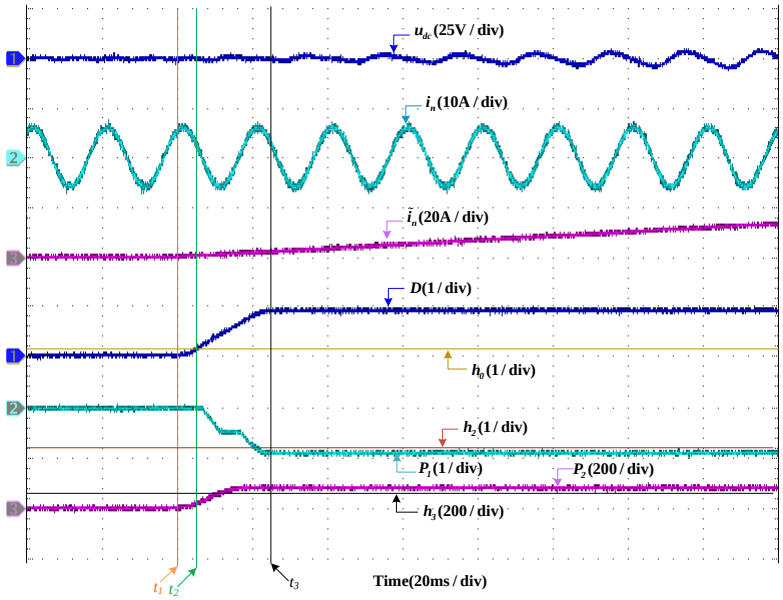

Figure 5. Fault diagnosis results of drift fault occurring in S_{Cn}.

The diagnosis results of S_{Cn} in a scaling fault are shown in Figure 6. It should be noted that the fault occurs at t_1. Then, u_{dc} decreases from 340 V over time. The fluctuation of $\tilde{i}_n$ becomes larger. After the fault occurs, D increases from 0 quickly, eventually reaching 1; when D surpasses h_0 at t_2, the fault is detected. P_1 grows rapidly from zero. The fault can be diagnosed when P_1 is bigger than h_1 at t_3.

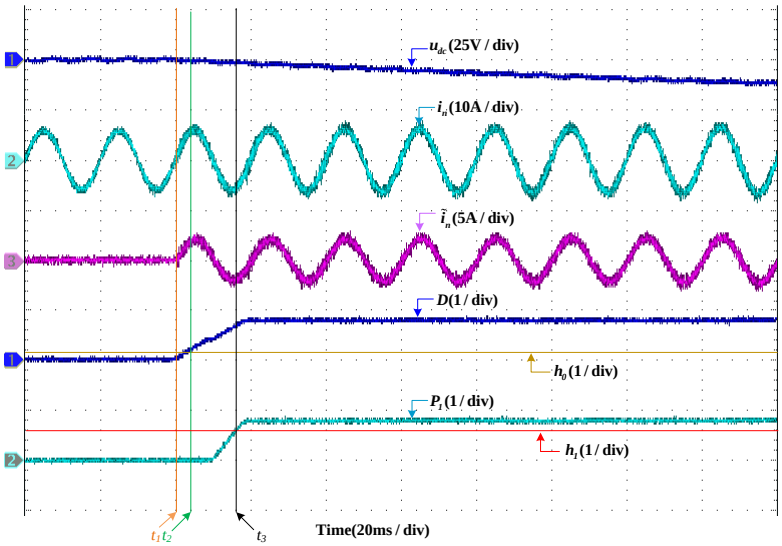

Figure 6. Fault diagnosis results of scaling fault occurring at in S_{Cn}.

The diagnosis results of S_{Vd} in the drift fault are shown in Figure 7. It should be noted that, after the fault occurs at t_1, due to the drift fault, the waveform of u_{dc} increases gradually. In a period of the system, it nearly reaches 344 V. i_n does not change obviously. $\tilde{i}_n$ changes from 0 and the amplitude of $\tilde{i}_n$ increases with time. D changes from 0 and eventually reaches 1. The fault can be detected when D surpasses h_0 at t_2. In the second half of the period of the system after the fault is detected, P_1 begins to fluctuate when the fault occurs, and P_1 is smaller than h_1 and bigger than h_2. P_2 is bigger than h_3 and keeps around 80. Then, after a period when the fault has been detected, it is diagnosed at t_3.

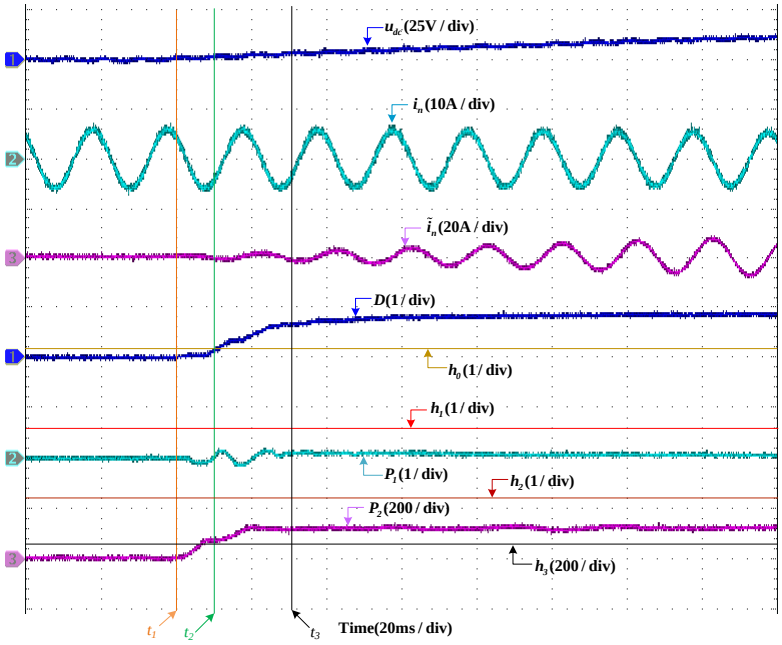

Figure 7. Fault diagnosis results of drift fault occurring in S_{Vd}.

Figure 8 shows the diagnosis results when S_{Vd} is an offset fault. It should be noted that after the fault occurs at t_1, the waveform of u_{dc} increases to 360 V, then, it decreases from 360 V gradually. The amplitude of i_n gets smaller, which nearly reaches 5 A. $\tilde{i}_n$ changes from 0 and nearly reaches 1, and the deviation of $\tilde{i}_n$ decreases with time. D changes from 0, and the fault can be detected when D surpasses h_0 at t_2. In the second half of the period of the system, P_1 begins to fluctuate when the fault occurs, and P_1 is smaller than h_1 and bigger than h_2. P_2 decreases to be less than h_3. Then, after a period when fault has been detected, it is diagnosed at t_3.

According to the theoretical analysis and experimental results, the performance of the proposed method could be compared with existing fault diagnosis methods, which is shown in Table 3.

Table 3. Comparison of fault diagnosis methods between previous methods and proposed method.

Fault Diagnosis Method	Object Sensor	Cost	Difficulty of Implementation	Fault Type
Fault diagnosis method in [23]	Only voltage sensor	Low	Low	Scaling & offset faults
Fault diagnosis method in [24]	Voltage & current sensor	Low	Low	Fault type is not identified
Fault diagnosis method in [25]	Voltage & current sensor	Low	Low	Offset fault
Fault diagnosis method in [26]	Only current sensor	Low	High	Fault type is not identified
Fault diagnosis method in [28]	Only voltage sensor	Low	High	Fault type is not identified
Fault diagnosis method in [29]	Only voltage sensor	High	Low	Fault type is not identified
Proposed method in paper	Voltage & current sensor	Low	Low	Scaling & offset & drift faults

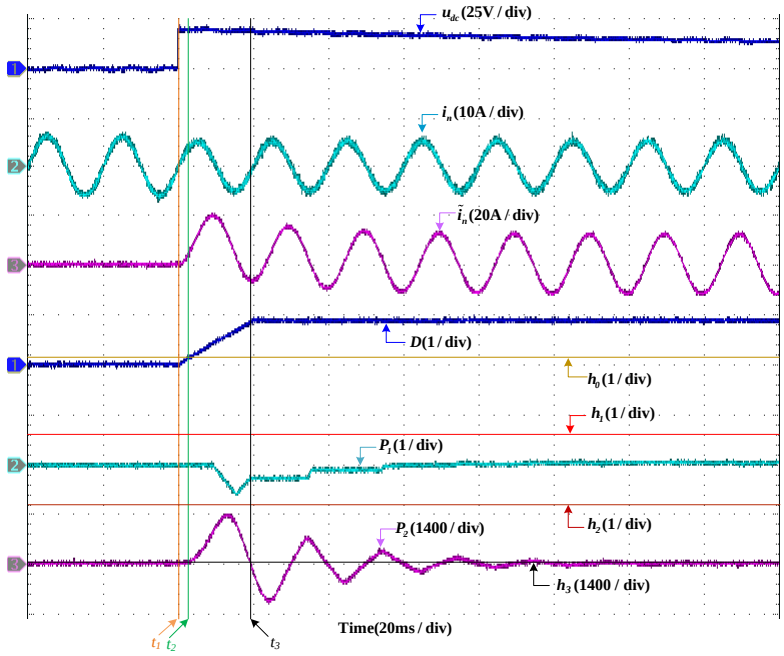

Figure 8. Fault diagnosis results of offset fault occurs in S_{Vd}.

6. Conclusions

The reliability of the single-phase rectifier plays a key role in the operation of a traction system. In order to avoid the control system failure when current or DC link voltage sensor faults occur, a new method is proposed. The offset, scaling and drift faults are high-incidence faults and influence the accuracy of feedback signals, which have been considered in the method. The residual of the current is acquired and analyzed. Experimental results verify the feasibility and effectiveness of the proposed method. The method does not need extra sensors, signals needed by the residual and the estimator are from the existing sensors. This method could be easily implemented, it also can improve the reliability of high-speed trains.

6.1. Limitation

This paper focused on three types of fault in sensors. Although the included faults are common, there are other kinds of fault may be considered. For example, due to the broken physics structure or the circuit of the sensor, the open loop fault may occurs in sensor. Besides, because the initial effect of the drift fault is tiny, the influence of the fault has been accumulated for a while, which may lead the detection time little longer than other fault. Because the diagnosis functions will locate the fault and identify fault type after fault has been detected, the structure of the diagnosis functions are a little complex.

6.2. Improvement for Future Works

The potential effects of other kinds of sensor fault should be taken into consideration in future works. Comprehensive fault types could improve the practicability and robustness of the diagnosis method. Due to the complex operation environment of traction system, the influence between the different parts of the traction system will be considered. This will contribute to guarantee reliability and improve the accuracy of this method. Furthermore, to ensure the safety of traction system and reduce the potential risk of sensor fault, the tolerant control will be included in the study. Study of fault tolerant control will also improve the integrity of the fault diagnosis method. Looking forward, further attempts have benefits to the corresponding research in field of fault diagnosis, and could also improve the reliability of electrical equipment of traction systems.

Author Contributions: Writing—original draft preparation, Y.Y., Y.S. and H.T.; writing—review and editing, Y.Y., Y.S., H.T. and J.H.; validation, Y.Y., Y.S. and H.T. All authors have read and agreed to the published version of the manuscript.

Funding: This work was supported in part by the Key Research and Development Program of Jiangxi Province-Research on Carbon Metabolism Optimization and Technology Integration for Carbon Peaking in Industrial Park under Grant 20214BBG74006, by the Program of Science and Technology Department of Jiangxi Province-Fault Prediction Based on Quantum Deep Learning for Photovoltaic Inverter under Grant ZBG20230418031, by the Key Research and Development Program of Jiangxi Province under Grant 20232BBG70031.

Data Availability Statement: Data are contained within the article.

Conflicts of Interest: The authors declare no conflict of interest.

References

1. Tao, H.; Peng, T.; Yang, C.; Gao, J.; Chen, Z.; Yang, C.; Gui, W. An FCS-MPC-based open-circuit and current sensor fault diagnosis method for traction inverters with two current sensors. *Int. J. Electr. Power Energy Syst.* **2023**, *144*, 108526. [CrossRef]
2. Peng, T.; Tao, H.; Yang, C.; Chen, Z.; Yang, C.; Gui, W.; Karimi, H.R. A Uniform Modeling Method Based on Open-circuit Faults Analysis For NPC-three-level Converter. *IEEE Trans. Circuits Syst. II Express Briefs* **2019**, *66*, 457–461. [CrossRef]
3. Cui, P.; Zheng, Z.; Fu, J.; Zhang, Q.; An, L. A Fault-Tolerant Control Method for a PMSM Servo Drive System with a Four-Leg Inverter. *Electronics* **2023**, *12*, 3857. [CrossRef]
4. Gong, Z.; Huang, D.; Jadoon, H.; Ma, L.; Song, W. Sensor-Fault-Estimation-Based Tolerant Control for Single-Phase Two-Level PWM Rectifier in Electric Traction System. *IEEE Trans. Power Electron.* **2020**, *35*, 12274–12284. [CrossRef]
5. Tao, H.; Peng, T.; Yang, C.; Chen, Z.; Yang, C.; Gui, W. Open-Circuit Fault Analysis and Modeling for Power Converter Based on Single Arm Model. *Electronics* **2019**, *8*, 633. [CrossRef]
6. Yang, X.; Yang, C.; Peng, T.; Chen, Z.; Liu, B.; Gui, W. Hardware in the Loop fault injection for traction control system. *IEEE J. Emerg. Sel. Top. Power Electron.* **2018**, *6*, 697–706. [CrossRef]
7. Ndabarushimana, E.; Ma, L. Robust Sensor Fault Detection for a Single-Phase Pulse Width Modulation Rectifier. *Electronics* **2023**, *12*, 2366. [CrossRef]
8. Zhou, D.; Ji, H.; He, X. Fault Diagnosis Techniques for the Information Control System of High-speed Trains. *Acta Anat. Sin.* **2018**, *44*, 1153–1164.
9. Tao, H.; Tao, P.; Yang, C.; Gao, J.; Yang, C.; Gui, W. Voltage and Current Sensor Fault Diagnosis Method for Traction Converter with Two Stator Current Sensors. *Sensors* **2022**, *22*, 2355. [CrossRef]
10. Xie, D.; Ge, X. A State Estimator-based Approach for Opencir-cuit Fault Diagnosis in Single-phase Cascaded H-bridge Rectifiers. *IEEE Trans. Ind. Appl.* **2019**, *55*, 1608–1618. [CrossRef]
11. Wu, F.; Zhao, J. Current Similarity Analysis Based Open-circuit Fault Diagnosis for Two-level Three-phase PWM Rectifier. *IEEE Trans. Power Electron.* **2017**, *32*, 3935–3945. [CrossRef]
12. Xie, D.; Pu, J.; Ge, X. Current Residual-based Method for Open-circuit Fault Diagnosis in Single-phase PWM Converter. *IET Power Electron.* **2018**, *11*, 2279–2285. [CrossRef]
13. Cheng, S.; Chen, Y.; Yu, T. A Novel Diagnostic Technique for Open-circuited Faults of Inverters Based on Output Line-to-line Voltage Model. *IEEE Trans. Ind. Electron.* **2016**, *63*, 4412–4421.
14. Cai, B.; Zhao, Y.; Liu, H. A Data-driven Fault Diagnosis Methodology in Three-phase Inverters for PMSM Drive Systems. *IEEE Trans. Power Electron.* **2017**, *32*, 5590–5600. [CrossRef]
15. Gou, B.; Xu, Y.; Xia, Y. An Intelligent Time-adaptive Data-driven Method for Sensor Fault Diagnosis in Induction Motor Drive System. *IEEE Trans. Ind. Electron.* **2019**, *66*, 9817–9827. [CrossRef]
16. Huang, G.; Zhou, H.; Ding, X. Extreme Learning Machine for Regression and Multiclass Classification. *IEEE Trans. Syst.* **2012**, *42*, 513–529.
17. Pecina Sánchez, J.A.; Campos-Delgado, D.; Espinoza-Trejo, D. Fault Diagnosis in Grid-Connected PV NPC Inverters by a Model-based and Data Processing Combined Approach. *IET Power Electron.* **2019**, *12*, 3254–3264. [CrossRef]
18. Foo, G.; Zhang, X.; Vilathgamuwa, D.M. A Sensor Fault Detection and Isolation Method in Interior Permanent-magnet Synchronous Motor Drives Based on an Extended Kalman filter. *IEEE Trans. Ind. Electron.* **2013**, *60*, 3485–3495. [CrossRef]
19. Jlassi, I.; Estima, J.; El Khil, S. A Robust Observer-Based Method for IGBTs and Current Sensors Fault Diagnosis in Voltage-source Inverters of PMSM Drives. *IEEE Trans. Ind. Appl.* **2017**, *53*, 2894–2905. [CrossRef]
20. Wu, C.; Guo, C.; Xie, Z.; Ni, F.; Liu, H. A Signal-Based Fault Detection and Tolerance Control Method of Current Sensor for PMSM Drive. *IEEE Trans. Ind. Electron.* **2018**, *65*, 9646–9657. [CrossRef]
21. Saha, S.; Kar, U. Signal-Based Position Sensor Fault Diagnosis Applied to PMSM Drives for Fault-Tolerant Operation in Electric Vehicles. *World Electr. Veh. J.* **2023**, *14*, 123. [CrossRef]
22. Xu, S.; Chai, H.; Hu, Y.; Huang, D.; Zhang, K.; Chai, Y. Simultaneous Fault Diagnosis of Broken Rotor Bar and Speed Sensor for Traction Motor in High-speed Train. *Zidonghua Xuebao* **2023**, *49*, 1214–1227.

23. Youssef, A.B.; Khil, S.; Belkhodja, I.S. Open-circuit fault diagnosis and voltage sensor fault tolerant control of a single phase pulsed width modulated rectifier. *Math. Comput. Simul.* **2017**, *131*, 234–252. [CrossRef]
24. Xia,J.; Guo, H.; Dai, B.; Zhang, X. Sensor fault diagnosis and system reconfiguration approach for an electric traction PWM rectifier based on sliding mode observer. *IEEE Trans. Power Electron.* **2017**, *53*, 4768–4778. [CrossRef]
25. Youssef, A.B.; Khil, S.; Slama-Belkhodja, I. State Observer-Based Sensor Fault Detection and Isolation, and Fault Tolerant Control of a Single-Phase PWM Rectifier for Electric Railway Traction. *IEEE Trans. Power Electron.* **2013**, *28*, 5842–5853. [CrossRef]
26. Li, Z.; Wheeler, P.; Watson, A.; Costabeber, A.; Wang, B.; Ren, Y.; Bai, Z.; Ma, H. A fast diagnosis method for both IGBT faults and current sensor faults in grid-tied three-phase inverters with two current sensors. *IEEE Trans. Power Electron.* **2020**, *35*, 5267–5278. [CrossRef]
27. Ren, Y.; Li, Z.; Wang, B.; Bai, Z.; Ma, H. A Fast Average Model-Based Method for IGBT and Current Sensor Fault Diagnosis in Grid-Tied Inverters. In Proceedings of the 44th Annual Conference of the IEEE Industrial Electronics Society, Washington, DC, USA, 21–23 October 2018; pp. 3809–3814.
28. Zhang, K.; Jiang, B.; Yan, X.; Mao, Z.H. Incipient Voltage Sensor for Rectifier in Railway Electrical Traction Systems. *IEEE Trans. Ind. Electron.* **2017**, *64*, 6763–6774. [CrossRef]
29. Li, X.; Xu, J.; Chen, Z.; Xu, S.; Liu, K. Real-time fault diagnosis of pulse rectifier in traction system based on structural model. *IEEE Trans. Intell. Transp. Syst.* **2020**, *23*, 2130–2143. [CrossRef]
30. Trinh, Q.; Wang, P.; Tang, Y.; Koh, L.; Choo, F. Compensation of DC Offset and Scaling Errors in Voltage and Current Measurements of Three-phase AC/DC Converters. *IEEE Trans. Ind. Electron.* **2018**, *33*, 5401–5414. [CrossRef]
31. Myoungho, K.; Seung-Ki, S.; Junggi, L. Compensation of Current Measurement Error for Current-Controlled PMSM Drives. *IEEE Trans. Ind. Appl.* **2014**, *550*, 3365–3373.

Disclaimer/Publisher's Note: The statements, opinions and data contained in all publications are solely those of the individual author(s) and contributor(s) and not of MDPI and/or the editor(s). MDPI and/or the editor(s) disclaim responsibility for any injury to people or property resulting from any ideas, methods, instructions or products referred to in the content.